Structural Heterogeneity and Ligand Binding in Carbonmonoxy Myoglobin Crystals at Cryogenic Temperatures†

G. Ulrich Nienhaus,*,‡ Kelvin Chu,§ and Klemens Jesse‡

Department of Physics, University of Illinois at Urbana-Champaign, 1110 West Green Street, Urbana, Illinois 61801-3080, Department of Biophysics, University of Ulm, D-89069 Ulm, Germany, and Los Alamos National Laboratory, Los Alamos, New Mexico 87545

Received November 19, 1997; Revised Manuscript Received March 2, 1998

ABSTRACT: We have characterized the ligand-rebinding behavior of single crystal native sperm whale carbonmonoxy myoglobin (swMbCO) (space group $P2_1$) and a synthetic mutant swMbCO (space group $P6$) at cryogenic temperatures by using temperature-derivative spectroscopy (TDS) with monitoring of the CO stretch bands in the mid-infrared. Crystals were studied at pH 5.1 and 7.0 for native swMbCO and at pH 7.0 for the mutant; both short-flash and extended illumination protocols were performed. The TDS analysis yields the enthalpy barrier distributions for recombination in the individual taxonomic (*A*) substates, A_0, A_1, and A_3. A single gaussian barrier distribution gave a good first-order description but was insufficient to precisely fit the data within each substate. An additional minority species was necessary to model the enhanced rebinding below 30 K, which likely appears because of quantum tunneling. The peak positions and widths of the enthalpy distributions are similar for the $P2_1$ and $P6$ crystal forms, indicating that crystal-packing forces have only very minor effects on the structure at the active site. Moreover, the widths of the (dominant) distributions are qualitatively similar to those observed with glycerol−water solutions, which shows that the degree of structural heterogeneity is similar for solution and crystalline samples. For the A_3 substate, a significantly lower peak enthalpy was obtained (by ∼4 kJ/mol) than for solutions, while the peak shifts in the A_0 and A_1 substates were small. In samples cooled under illumination, discrete populations with higher rebinding barriers were observed. Concomitant changes in the stretch absorption of the photodissociated CO (*B* states) only occur between 100 and 130 K. They likely arise from movements of the ligand in the heme pocket between discrete sites.

Ligand binding to heme proteins is a simple model reaction for understanding the fundamental concepts of protein dynamics (*1*). Often carbonmonoxy myoglobin (MbCO) is used in these studies, and the rebinding following photolysis reveals an impressive complexity for this apparently simple reaction, in both theory (*2*) and experiment (*3*). The complex behavior of this relatively small biomolecule arises from its ability to assume a large number of slightly different conformational substates within its conformations (*4*).

Despite substantial efforts, the structural changes that accompany ligand binding and dissociation are still not well understood. New data on the events that occur immediately after photodissociation of CO from myoglobin have been provided by femtosecond infrared measurements by Lim et al. (*5, 6*), low-temperature X-ray structures of the Mb*CO photoproduct reported by Schlichting et al. (*7*), Teng et al. (*8, 9*), and Hartmann et al. (*10*), and recently, a nanosecond time-resolved X-ray structure analysis after laser flash photolysis (*11*). Cryocrystallography is a particularly revealing technique to observe ligand-binding reactions in detail because the reduced binding rates at low temperatures allow one to prepare significant populations of reaction intermediates. Moreover, *B* factors are reduced, and sample degradation due to laser excitation and X-rays may be avoided. In principle, the resulting high-quality electron density maps allow one to pinpoint even subtle structural changes that can, nevertheless, strongly affect the ligand binding reaction.

It is essential for the interpretation of the measured X-ray structures that the ligand-binding kinetics under the given experimental conditions be known. Indeed, discrepancies in two different low-temperature photoproduct structures (*7, 8*) have been suggested to arise from different ligand-binding properties in the crystals under the chosen experimental conditions (*10*). So far, only very little quantitative information is available on low-temperature ligand binding to heme proteins in the crystalline environment (*3*), as traditionally, those experiments have preferentially been carried out in glycerol−water solvents (*12, 13*), owing to their superior optical properties. However, it is not a priori clear that the ligand-binding properties of solutions and crystals are similar, as proteins respond sensitively to their environment, and the intermolecular contacts and high salt concentrations in protein crystals could lead to significant changes.

Here, we present kinetic data on ligand recombination after photodissociation in MbCO crystals at low temperature. This information not only helps to interpret the previously performed cryocrystallographic studies (*7*−*10*) but also allows one to choose optimal experimental parameters, especially pH and temperature, in cryocrystallographic

† This work was supported in part by the National Institutes of Health (Grant GM 18051) and the National Science Foundation (Grant PHY95-13217).

* Author to whom correspondence should be addressed; University of Ulm and University of Illinois.

‡ University of Ulm.

§ Los Alamos National Laboratory.

S0006-2960(97)02843-2 CCC: $15.00
Published on Web 04/23/1998

experiments to elucidate further details of the reaction pathway. We have performed temperature-derivative spectroscopy (TDS) (*14*) using the IR stretch bands of bound and photodissociated carbon monoxide in crystals of native MbCO (space group $P2_1$) and a mutant MbCO that crystallizes in the *P*6 space group (*15*). Monitoring of the stretch absorption of the CO ligands in the mid-infrared allows us to obtain the kinetics of the individual taxonomic (*A*) substates of MbCO and also to observe changes in the stretch absorption of the photodissociated CO, which signal movement of the ligand in the heme pocket (*3*, *4*).

MATERIALS AND METHODS

Sample Preparation. Met-myoglobin crystals, kindly provided by Drs. F. G. Parak and G. N. Phillips, Jr., were reduced anaerobically with sodium dithionite under a CO atmosphere. Crystalline infrared samples were prepared by crushing small crystals between two sapphire windows kept apart by a 50 μm mylar donut spacer. Samples were cooled down to 12 K immediately after preparation.

FTIR Cryospectroscopy. Transmittance spectra were collected on a Fourier transform infrared (FTIR) spectrometer (model Sirius 100, Mattson, Madison, WI) between 1800 and 2300 cm^{-1} with a resolution of 2 cm^{-1}. For each spectrum, 400 mirror scans were taken in 320 s.

The samples were kept in a block of oxygen-free high conductivity copper mounted on the cold-finger of a closed-cycle helium refrigerator (model 22C, CTI Cryogenics, Waltham, MA), regulated with a digital temperature controller (model DRC93C, Lake Shore Cryotronics, Westerville, OH).

Sample illumination was done with light from an argon ion laser (Omnichrome, model 543, Chino, CA), operated at 300 mW multimode output. It emitted predominantly at 488 and 514 nm. The beam was split and focused with lenses on the crystalline samples from both sides. Standard TDS measurements (vide infra) were started after complete photodissociation by illuminating the samples for 5 s at a photolysis rate of 5 s^{-1}. For light-induced relaxation (LIR) experiments, samples were cooled from 200 to 12 K at a rate of 10 K/h while being illuminated with a photolysis rate of 20 s^{-1}.

Temperature-Derivative Spectroscopy. TDS is an efficient method to obtain kinetic information on thermally activated processes. Here, we sketch only the basic idea, details have been given earlier (*3*, *14*, *16*). In a TDS experiment, the sample is photodissociated at the lowest achievable temperature, in our experiments 12 K. The temperature is then increased linearly in time, so that the ramp temperature, T_R, is given by

$$T_R(t) = T_{min} + \alpha t \tag{1}$$

where α= 5.0 mK/s is the heating rate in the present experiments. Spectra are collected continuously at fixed temperature intervals (here we collected one spectrum for every kelvin). At low temperatures, only molecules with small barriers recombine. With increasing temperature (and time), molecules with successively higher barriers recombine, and the changes between successive spectra represent the fraction of molecules that have rebound during that time and temperature interval. Assuming that the Arrhenius law describes the temperature dependence of the recombination rate, the negative derivative of the photolyzed fraction with respect to the temperature, $-dN/dT_R$, closely resembles the distribution of rebinding barriers, $g(H_{BA})$. The quantitative analysis involves a non-linear least-squares fit of (usually gaussian) model distributions to the TDS signal, $-dN/dT_R$ (*14*).

To approximate the derivative, absorbance difference spectra, $\Delta A(\upsilon,T_R)$, are calculated from transmittance spectra, $I(\upsilon,T_R)$, at consecutive temperatures,

$$\frac{dA}{dT_R} \approx \Delta A(\upsilon,T_R) = \log I\left(\upsilon,T_R - \frac{1}{2}K\right) - \log I\left(\upsilon, T_R + \frac{1}{2}K\right) \tag{2}$$

Taking the absorbance to be proportional to the concentration of the photolyzed species and normalizing yields, $-dN/dT_R$. We present TDS data in two different ways: either as contour maps of $\Delta A(\upsilon,T_R)$ or as integrated absorbances, $\Delta A(T_R)$, as a function of T_R by integrating over the wavenumber region spanned by a particular spectroscopic line.

TDS measures rebinding as a function of the ramp temperature T_R. To convert T_R into an activation enthalpy, we use the fact that geminate rebinding is a first-order process and can be described by an Arrhenius relation. T_R and the rebinding enthalpy, *H*, are related by (*14*)

$$H = RT_R \ln(A\tau_c), \tag{3}$$

where the characteristic time τ_c is given by

$$\tau_c = \frac{RT_R^3}{\alpha T_0(H + RT_R).} \tag{4}$$

Here, T_0 = 100 K is a reference temperature. If the pre-exponential, *A*, is known, eqs 3 and 4 can be solved numerically to connect *H* and T_R.

RESULTS AND DISCUSSION

In Figure 1, TDS contour plots for the monoclinic crystal sample at pH 7.0 and 5.1 (panels a and b) and for the hexagonal crystal at pH 7.8 (panel c) are shown, representing the absorption changes of the infrared spectra as a function of frequency and the ramp temperature T_R at which the changes occur. In all three data sets, three different spectroscopic bands are seen at roughly 1966, 1945, and 1930 cm^{-1}, corresponding to the A_0, A_1, and A_3 taxonomic substates (*4*, *17*). Their characteristic absorption frequencies arise from different electrostatic interactions between the bound CO and its heme pocket environment (*6*−*24*). While A_0 is only weakly populated at high pH (Figure 1, panels a and c), it is much stronger in the low-pH sample in Figure 1b. X-ray structures by Yang and Phillips (*25*) have shown that the transition to the A_0 substate involves a conformational change where the imidazole side chain of the distal histidine (H64) rotates and points toward the solvent in response to protonation of the imidazole at low pH. Note that the high-pH data in Figure 1, panels a and c, look very similar, implying that the different crystal-packing forces in the two space groups do not have a marked influence on the recombination properties at low temperatures.

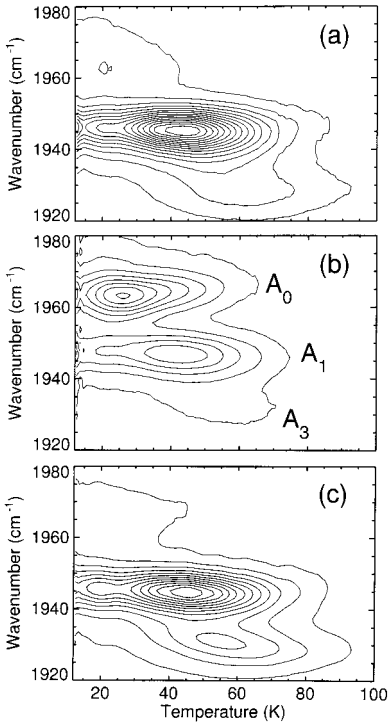

FIGURE 1: TDS maps of ligand rebinding to Mb following photolysis at low temperature. The three *A* substates are labeled in panel b. (a) Monoclinic ($P2_1$) MbCO, pH 7.0. (b) Monoclinic MbCO, pH 5.1. (c) Hexagonal (*P*6) MbCO, pH 7.0. The contours are spaced linearly.

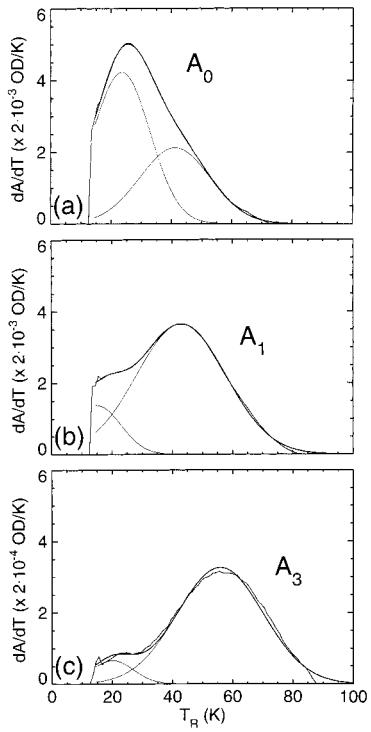

FIGURE 2: Integrated absorbances for the *A* states ($P2_1$ crystals, pH 5.1) with decomposition into gaussian subpopulations. Fit parameters are given in Table 1. (a) A_0, (b) A_1 and (c) A_3.

Rebinding within each *A* substate occurs over an interval of several 10 K. This observation implies that, even in the highly ordered crystalline arrangement, there are molecules that have small rebinding barriers, enabling them to recombine at, e.g., 20 K, whereas in others, the barriers are significantly larger, so that they rebind only above 80 K. For MbCO solutions at cryogenic temperatures, this functional heterogeneity has been known for a long time (*12*). It is surprising that the low-temperature rebinding properties in crystals are qualitatively similar to those found in solution experiments (*3*).

For a quantitative analysis, the TDS signals for the three *A* substates were integrated and the absorbances fitted with gaussian enthalpy distributions. Figure 2 shows the data for the three *A* substates in the pH 5.1 sample, together with the fit using a sum of two gaussian enthalpy distributions. The fit parameters for all three samples in Figure 1 are listed in Table 1. Maximum rebinding of A_3 occurs at ~55 K. Using the pre-exponential of $10^{10.4}$ s^{-1} from kinetic experiments (*17*), the barrier distributions are well fitted by a gaussian centered at ~14 kJ/mol, which is significantly less than the 18.3 kJ/mol reported for glycerol−water mixtures (*17*). The single-gaussian fit misses on the low-temperature tail, and the minority population of proteins rebinding at low temperatures can be accounted for by a second gaussian with a peak enthalpy below 5 kJ/mol (see Figure 2b). The A_1 substate has a peak enthalpy between 9.1 and 9.6 kJ/mol, slightly less than the 10.0 kJ/mol in glycerol−water solutions. Again, a minor fraction of the population (between 7 and 15%) with small barriers exists that can be modeled with a gaussian enthalpy distribution peaking around 3 kJ/mol, as shown in the contour plot in Figure 1 c. In the A_0 substate, a single gaussian enthalpy distribution cannot model the data either. The high-pH samples, like solution samples (*3*), show a tailing of the population toward high temperatures; only the low-pH sample shows a clear maximum. The fraction of molecules that rebind below 30 K (barriers smaller than 6−7 kJ/mol) is much more pronounced than in A_1 and A_3 and not only a small correction to the overall distribution. Therefore, it is not possible to cleanly separate two distinct distributions within A_0. The parameters in Table 1 are the best-fit results; we emphasize, however, that different combinations of two gaussians give acceptable agreement with the data.

The additional minority species present in the data of A_1 and A_3 arise, at least partially, from a quantum tunneling effect, which leads to enhanced rebinding at low temperature following photolysis (*26*). Note that the TDS analysis used here assumes a thermally activated (Arrhenius) first-order reaction and thus cannot model tunneling processes adequately. While this is of minor relevance in the A_1 and A_3 substates, tunneling may play a more important role in the recombination in the A_0 substate.

Recent work on MbCO solutions at cryogenic temperatures has revealed that the barrier distributions reported in Table 1 are present when only a small number of light quanta impinge on each molecule and that prolonged illumination can dramatically slow the rebinding of CO due to increased enthalpic barriers (*16*). This process is known as light-induced relaxation (LIR), and similarities have been noted to the thermal relaxation after photodissociation in flash-photolysis experiments (*13*, *27*, *28*). As part of the effort to explore the consequences of different illumination protocols in cryocrystallography of photoproduct structures, we have also investigated the effect of LIR on both the $P2_1$ and *P*6 crystals. The experiments show that crystals exhibit overall similar behavior as the glycerol−water solutions (*16*), but

Table 1: Parameters for Ligand Binding to MbCO at Low Temperatures[a]

sample	*A* substate	log(*A*/s^{-1})	C_1	H_{p1} (kJ/mol)	$H_{\sigma 1}$ (kJ/mol)	C_2	H_{p2} (kJ/mol)	$H_{\sigma 2}$ (kJ/mol)
$P2_1$, pH 7.0	A_0	8.7	0.68	3.1	2.7	0.32	9.0	3.2
	A_1	8.9	0.07	3.2	1.1	0.93	9.5	3.6
	A_3	10.4	0.02	4.2	1.2	0.98	14.9	4.6
$P2_1$, pH 5.1	A_0	8.7	0.65	4.7	2.1	0.35	8.8	2.5
	A_1	8.9	0.15	3.0	1.6	0.85	9.1	3.4
	A_3	10.4	0.08	4.6	1.7	0.92	13.8	3.8
*P*6, pH 7.8	A_0	8.7	0.45	2.7	2.5	0.55	5.5	4.8
	A_1	8.9	0.10	3.3	1.1	0.90	9.6	3.7
	A_3	10.4	0.02	4.0	1.3	0.98	14.6	4.4

[a] The TDS integrated absorbances, as shown for the crystals at pH 5.1 in Figure 2, were fitted with a sum of two gaussian enthalpy distributions, $g(H) = \sum_{i=1,2} C_i (2\pi H_{\sigma i}^2)^{-1/2} \exp[-(H - H_{pi})2/(2H_{\sigma i}^2)$ (*14*). The preexponential factors, *A*, were taken from isothermal flash photolysis experiments (*17*).

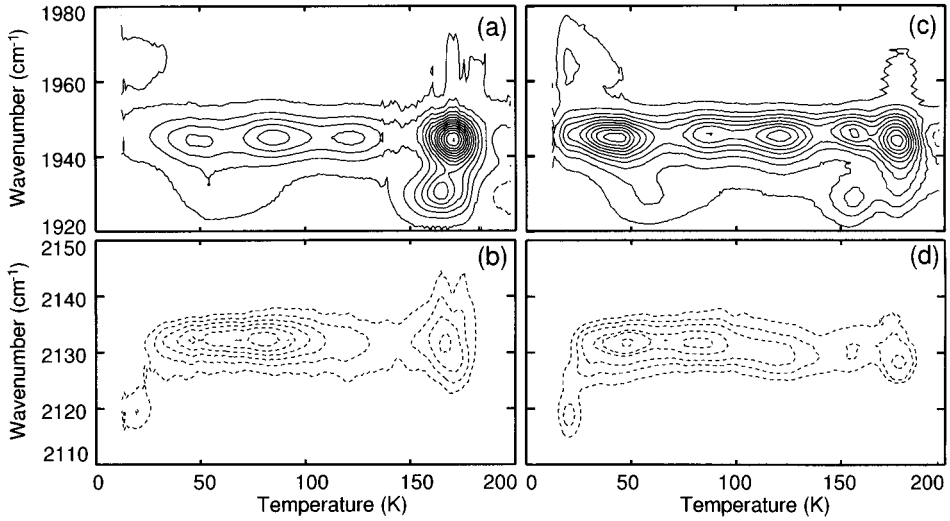

FIGURE 3: Light-induced relaxation (LIR) in the hexagonal and monoclinic forms. (a) Hexagonal, *A* states. (b) Hexagonal, *B* states. (c) Monoclinic, *A* states, (d) Monoclinic, *B* states. Note the pronounced shift in the *B* substates above 100 K in panel d. The contours are spaced linearly.

differ in detail. The *A* substate TDS maps after illumination under slow cooling from 200 to 12 K are shown in Figure 3, panels a and c, for the *P*6 and $P2_1$ space groups, respectively. While upon short illumination at 12 K, rebinding is completed by 100 K, we see that, after extended illumination, rebinding continues up to 200 K as a series of discrete populations. We note that, if instead of slow cooling, illumination at constant temperature is used, long-lived populations are created that rebind near the temperature of illumination; details can be found in ref *16*.

For both space groups, rebinding above 150 K is observed for all three *A* substates. Particularly pronounced is the population in A_1 in the *P*6 data at 170 K. The underlying barrier distribution is narrow (less than 2 kJ/mol), which suggests that fluctuational averaging of the barrier distribution occurs on the characteristic time scale of the TDS experiment (∼100 s) (*14*). The fact that the A_1 and A_3 recombination peaks appear at slightly different temperatures indicates, however, that interconversion between the taxonomic substates is still slow below 170 K in crystals. Below 150 K, A_0 and A_3 do not show significant slowing of the rebinding, in agreement with the low yields of LIR in glycerol−water solutions (*16*). A_1 in the *P*6 crystal also has three peaks below 150 K, as in solution. The *A* state TDS map for the $P2_1$ crystal form (Figure 3c) looks overall very similar to that for the *P*6 form except for the appearance of an additional rebinding population at 157 K in A_1 and A_3.

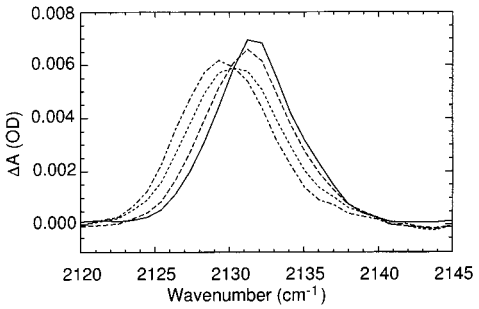

FIGURE 4: Normalized consecutive differences over the $P2_1$ LIR TDS map at 100, 110, 120, and 130 K (from right to left), displaying interconversion between two *B* substates.

This new process is likely due to a protein relaxation that is allowed in the $P2_1$ form but discouraged in the *P*6 form by differences in crystal contacts (*15*).

The concomitant maps for the unbound, or *B*, states are shown in Figure 3, panels b and d. In both maps, rebinding occurs predominantly through the *B* state at 2132 cm^{-1} [assigned in solution studies as *B*2131 (*3*)]. At higher temperatures (T > 100 K) in the $P2_1$ crystal, Figure 3d, a transition to a line at 2128 cm^{-1} is observed, as indicated by the isosbestic point at 2130 cm^{-1} (Figure 4). Because the CO stretch frequency is sensitive to the local electrostatic environment (*6*−*24*), the state at lower wavenumber represents most likely an alternative ligand position in the pocket that is distinguishable in the $P2_1$ crystal spectra. The narrow

B state lines observed here support the presence of discrete docking sites of the photodissociated CO, as is also implied by the femtosecond infrared work at room temperature (*5*, *6*). The data presented here should be useful for refining the molecular dynamics simulations of the photodissociated CO in the heme pocket (*24*, *29*).

In a recent paper, Teng et al. (*9*) reported X-ray diffraction studies of MbCO at 40 K showing the ligand migrating away from the active site upon extended illumination. While our spectroscopic data do not allow us to make definitive statements on structural aspects, we emphasize that it is only above 100 K that we see pronounced spectral shifts that may arise from ligand motion. For MbCO solutions, we have shown that extended illumination in the temperature range below 50 K yields no spectral changes in the *B* state bands or band III in the near-infrared and only small changes in the barrier distributions (*16*), even for photon numbers 10-fold larger than those reported in the X-ray studies (*9*). The (apart from details) analogous behavior of crystals observed here raises the question if the CO stretch absorption is indeed insensitive to ligand movements by almost 2 Å in the heme pocket at 40 K, as proposed by Teng et al. (*9*). However, low-temperature structure determination of photoproducts is still a challenging task, as reflected in the differences among the various structures (*7*−*10*), and one should also critically assess the limitations of these studies. For example, it has not yet become possible to resolve the structural differences of the *A* substates, although they are obviously present in crystals (Figures 1−3). Moreover, with crystals containing significant fractions of aquomet myoglobin (*8*, *9*), it is difficult to separate this species from the CO-ligated and deligated form, and photodissociation of the water ligand after photoreduction of the heme iron by X-rays could possibly create additional complications (*30*).

CONCLUSIONS

We have shown that ligand rebinding in swMbCO in the $P2_1$ and $P6$ crystal forms at cryogenic temperatures is qualitatively similar to that observed in solution experiments. To obtain a completely photodissociated sample, crystals at high pH should be used to avoid the presence of the low-barrier A_0 population. In samples subjected to extended illumination, discrete populations with higher rebinding barriers are created in a similar way as in solution samples. With X-ray diffraction experiments of MbCO crystals after prolonged illumination at the appropriate temperatures it will be possible to elucidate the structural changes that drastically alter the ligand binding properties.

ACKNOWLEDGMENT

We thank Drs. G. N. Phillips, Jr., and F. G. Parak for providing the myoglobin crystals used in this study and D. C. Lamb and S. S. Stavrov for fruitful discussions. K.C. wishes to acknowledge a LANL Directors Funded Postdoctoral Fellowship and K.J. a postdoctoral fellowship of the Graduiertenkolleg “Molekulare Organisation und Dynamik an Grenz- und Oberflächen” for support.

REFERENCES

1. Antonini, E., and Brunori, M. (1971) *Hemoglobin and Myoglobin in their Reactions with Ligands*, North-Holland, Amsterdam.
2. Elber, R., and Karplus, M. (1990) *J. Am. Chem. Soc. 112*, 9161−9175.
3. Mourant, J. R., Braunstein, D. P., Chu, K., Frauenfelder, H., Nienhaus, G. U., Ormos, P., and Young, R. D. (1993) *Biophys. J. 65*, 1496−1507.
4. Frauenfelder, H., Sligar, S. G., and Wolynes, P. G. (1991) *Science 254*, 1598−1603.
5. Lim, M., Jackson, T. A., and Anfinrud, P. A. (1996) J. *Phys. Chem. 100*, 12043−12051.
6. Lim, M., Jackson, T. A., and Anfinrud, P. A. (1997) *Nat. Struct. Biol. 33*, 209−214.
7. Schlichting, I., Berendzen, J., Phillips, G. N., Jr., and Sweet, R. M. (1994) *Nature 371*, 808−812.
8. Teng, T., Srajer, V., and Moffat, K. (1994) *Nat. Struct. Biol. 1*, 701−705.
9. Teng, T., Srajer, V., and Moffat, K. (1997) *Biochemistry 36*, 12087−12100.
10. Hartmann, H., Zinser, S., Komninos, P., Schneider, R. T., Nienhaus, G. U., and Parak, F. (1996) *Proc. Natl. Acad. Sci. U.S.A. 93*, 7013−7016.
11. Srajer, V., Teng, T., Ursby, T., Pradervand, C., Ren, Z., Adachi, S., Schildkamp, W., Bourgeois, D., Wulff, M., and Moffat, K. (1996) *Science 274*, 1726−1729.
12. Austin, R. H., Beeson, K. W., Eisenstein, L., Frauenfelder, H., and Gunsalus, I. C. (1975) *Biochemistry 14*, 5355−5373.
13. Steinbach, P. J., Ansari, A., Berendzen, J., Braunstein, D., Chu, K., Cowen, B. R., Ehrenstein, D., Frauenfelder, H., Johnson, J. B., Lamb, D. C., Luck, S., Mourant, J. R., Nienhaus, G. U., Ormos, P., Philipp, R., Xie, A., and Young, R. D. (1991) *Biochemistry 30*, 3988−4001.
14. Berendzen, J., and Braunstein, D. (1990) *Proc. Natl. Acad. Sci. U.S.A. 87*, 1−5.
15. Phillips, G. N., Jr. (1990) *Biophys. J. 57*, 381−383.
16. Nienhaus, G. U., Mourant, J. R., Chu, K., and Frauenfelder, H. (1994) *Biochemistry 33*, 13413−13430.
17. Johnson, J. B., Lamb, D. C., Frauenfelder, H., Müller, J. D., McMahon, B. H., Nienhaus, G. U., and Young, R. D. (1996) *Biophys. J. 71*, 1563−1573.
18. Park, K. D., Guo, K., Adebodun, F., Chiu, M. L., Sligar, S. G., and Oldfield, E. (1991) *Biochemistry 30*, 2333−2347.
19. Straub, J. E., and Karplus, M. (1991) *Chem. Phys. 158*, 221−248.
20. Braunstein, D. P., Chu, K., Egeberg, K. D., Frauenfelder, H., Mourant, J. R., Nienhaus, G. U., Ormos, P., Sligar, S. G., Springer, B. A., and Young, R. D. (1993) *Biophys. J. 65*, 2447−2454.
21. Li, T., Quillin, M. L., Phillips, G. N., Jr., and Olson, J. S. (1994) *Biochemistry 33*, 1433−1446.
22. Ray, G. B., Li, X. Y., Ibers, J. A., Sessler, J. L., and Spiro, T. G. (1994) *J. Am. Chem. Soc. 116*, 162−176.
23. Kushkuley, B., and Stavrov, S. S. (1996) *Biophys. J. 70*, 1214−1229.
24. Ma, J., Huo, S., and Straub, J. E. (1997) *J. Am. Chem. Soc. 119*, 2541−2551.
25. Yang, F., and Phillips, G. N., Jr. (1996) *J. Mol. Biol. 256*, 762−774.
26. Alben, J. O., Beece, D., Bowne, S. F., Eisenstein, L., Frauenfelder, H., Good, D., Marden, M. C., Moh, P. P., Reinisch, L., Reynolds, A. H., and Yue, K. T. (1980) *Phys. Rev. Lett. 44*, 1157−1160.
27. Agmon, N., and Hopfield, J. J. (1983) *J. Chem. Phys. 79*, 2042−2053.
28. Chu, K., Ernst, R. M., Frauenfelder, H., Mourant, J. R., Nienhaus, G. U., and Philipp, R. (1995) *Phys. Rev. Lett. 74*, 2607−2610.
29. Vitkup, D., Petsko, G. A., and Karplus, M. (1997) *Nat. Struct. Biol. 34*, 202−208.
30. Lamb, D. C., Prusakov, V. E., Engler, N., Ostermann, A., Schellenberg, P., Parak, F. G., and Nienhaus, G. U. (1998) *J. Am. Chem. Soc. 120* (in press).

BI972843H